Published in final edited form as:
Mol Imaging Biol. 2013 August ; 15(4): . doi:10.1007/s11307-013-0610-6.

IMPROVED DERIVATION OF INPUT FUNCTION IN DYNAMIC MOUSE [^{18}F]FDG PET USING BLADDER RADIOACTIVITY KINETICS

Koon-Pong Wong[1], **Xiaoli Zhang**[1], and **Sung-Cheng Huang**[1,2]

[1]Department of Molecular and Medical Pharmacology, David Geffen School of Medicine at UCLA, Los Angeles, California.

[2]Department of Biomathematics, David Geffen School of Medicine at UCLA, Los Angeles, California.

Abstract

Purpose—Accurate determination of the plasma input function (IF) is essential for absolute quantification of physiological parameters in positron emission tomography (PET). However, it requires an invasive and tedious procedure of arterial blood sampling that is challenging in mice because of the limited blood volume. In this study, a hybrid modeling approach is proposed to estimate the plasma IF of 2-deoxy-2-[^{18}F]fluoro-D-glucose ([^{18}F]FDG) in mice using accumulated radioactivity in urinary bladder together with a single late-time blood sample measurement.

Methods—Dynamic PET scans were performed on nine isoflurane-anesthetized male C57BL/6 mice after a bolus injection of [^{18}F]FDG at the lateral caudal vein. During a 60- or 90-min scan, serial blood samples were taken from the femoral artery. Image data were reconstructed using filtered backprojection with CT-based attenuation correction. Total accumulated radioactivity in the urinary bladder was fitted to a renal compartmental model with the last blood sample and a 1-exponential function that described the [^{18}F]FDG clearance in blood. Multiple late-time blood sample estimates were calculated by the blood [^{18}F]FDG clearance equation. A sum of 4-exponentials was assumed for the plasma IF that served as a forcing function to all tissues. The estimated plasma IF was obtained by simultaneously fitting the [^{18}F]FDG model to the time-activity curves (TACs) of liver and muscle and the forcing function to early (0–1 min) left-ventricle data (corrected for delay, dispersion, partial-volume effects and erythrocytes uptake) and the late-time blood estimates. Using only the blood sample acquired at the end of the study to estimate the IF and the use of liver TAC as an alternative IF were also investigated.

Results—The area under the plasma TACs calculated for all studies using the hybrid approach was not significantly different from that using all blood samples. [^{18}F]FDG uptake constants in brain, myocardium, skeletal muscle and liver computed by the Patlak analysis using estimated and measured plasma TACs were in excellent agreement (slope ~ 1; $R^2 > 0.938$). The IF estimated using only the last blood sample acquired at the end of the study and the use of liver TAC as plasma IF provided less reliable results.

Address for correspondence: Koon-Pong Wong, PhD, Department of Molecular and Medical Pharmacology, David Geffen School of Medicine at UCLA, Rm. B2-085E CHS, 10833 Le Conte Avenue, Los Angeles, CA 90095, USA, Tel: (310) 825 7985, Fax: (310) 825 4517, kpwong@ucla.edu.

Portions of this work were presented at the IEEE Medical Imaging Conference, Dresden, Germany, October 22-25, 2008 and the 56th Annual Meeting of the Society of Nuclear Medicine, Toronto, Canada, June 13-17, 2009.

CONFLICT OF INTEREST DISCLOSURE

The authors declare that they have no conflict of interest.

Conclusions—The estimated plasma IFs obtained with the hybrid model agreed well with those derived from arterial blood sampling. Importantly, the proposed method obviates the need of arterial catheterization, making it possible to perform repeated dynamic [^{18}F]FDG PET studies on the same animal. Liver TAC is unsuitable as an input function for absolute quantification of [^{18}F]FDG PET data.

Keywords

arterial input function; renal modeling; [^{18}F]FDG; dynamic imaging; mouse; urinary bladder

INTRODUCTION

Positron emission tomography (PET) is increasingly used in animal models of various human diseases. In particular, the 2-deoxy-2-[^{18}F]fluoro-D-glucose ([^{18}F]FDG) PET technique that has been used for the *in vivo* measurement of local glucose utilization in man, is playing a pivotal role in rodent models and transgenic mice to study human diseases and tissue responses due to various drug treatments and therapies. Absolute quantification of glucose utilization rate in a local tissue requires either an operational equation calculated along with a predefined set of rate constants when only a single static scan is performed at a specific time postinjection [1] or compartmental/graphical analysis on the time course of tissue kinetics acquired with dynamic imaging [2, 3]. Inherent in these methods is an invasive and tedious blood sampling procedure to measure the [^{18}F]FDG activity concentration in arterial plasma at timed intervals during the uptake/imaging period to form the *input function* (IF) for kinetic analysis [4]. While direct blood sampling is considered the reference standard for determination of the IF, the procedure is technically challenging in rodents because of the small caliber of blood vessels and the limited total blood volume.

Several alternative methods for the derivation of IF have been proposed for [^{18}F]FDG PET studies in humans and small animals. These methods include arteriovenous shunting [5, 6], β-microprobe measurement [7, 8], automatic micro-blood-sampling system [9], population-averaged measurement [10, 11], image-derived measurement from a large vascular structure [12–17], model-based estimation [18–20] and a combination of the last two approaches [21–23]. Although the use of arteriovenous shunts [5, 6] or automatic micro-blood-sampling system [9] may allow minimization of blood loss and standardization of blood sampling protocol, they require a time-consuming and invasive surgical procedure to implant the catheters, making these techniques not possible for use in repetitive study on the same animal. Likewise, the β-microprobe technique [7, 8] has similar issues as an invasive microsurgery is needed to expose the blood vessel so that the β-microprobe can be positioned inside or in direct contact with the blood vessel. The size of the β-microprobe, which needs to be small when comparing to the blood vessel, has also limited the technique be applicable to rat studies so far [7]. Population-based method [10, 11] calibrates a standardized IF obtained from a large population by one to two blood samples for an individual by assuming that the shape of the IF is identical among subjects and groups. However, the shape discrepancies in the IF resulting from different injection rates or study conditions can cause erroneous estimation of physiological parameters. Repeated measurements in a group of subjects are required for constructing a new IF template whenever a new tracer or different injection schedule is used or when a different physiological condition of the animals is studied. Derivation of IF from region-of-interest (ROI) defined manually over a vascular structure on the PET images [12–14] or by means of multivariate statistical approaches [15–17] has also been investigated. Due to the limited spatial resolution of PET and the small size of the vascular ROI, the image-derived IF is prone to partial-volume and spillover effects and its noise level cannot be assumed to be negligible for kinetic modeling. In this context, a model-based approach such as

simultaneous estimation (SIME) method [18, 19] has been proposed to simultaneously estimate, with the aid of one or two late-time blood samples for scaling purpose, the kinetic parameters in multiple tissue ROIs and the underlying plasma IF, which can be parameterized by a mathematical model. This approach has recently been extended to small-animal [^{18}F]FDG PET studies [21–23] with reduced number of parameters to be estimated and improved identifiability of the estimated IF using an image-derived time-activity curve (TAC) from the left ventricle (LV).

Nevertheless, it has been shown in all those studies that at least one blood sample is required to scale the estimated IF and determine the plasma glucose level. Therefore, taking a blood sample appears to be unavoidable for [^{18}F]FDG PET. However, we speculate that pharmacokinetic parameters equivalent to data from full blood sampling can be obtained if one can utilize this single blood sample measurement and take other physiological information into account. We have recently shown in mice that [^{18}F]FDG clearance rate in plasma is strongly correlated with [^{18}F]FDG accumulation rate in urinary bladder [24]. In this study, we propose a hybrid modeling approach that based partially on the renal physiology to estimate the plasma curve at late times by use of the total accumulated radioactivity in the urinary bladder and the blood sample collected at the end of the PET experiment and we validate it with dynamic mouse [^{18}F]FDG PET data. The results of IF estimation are expected to be improved when comparing to those using only one blood sample withdrawn at the end of the PET study as extra physiological information is incorporated into the estimation process. The use of liver TAC as an alternative IF is also investigated and the results are compared to those obtained with the proposed hybrid approach and the gold standard method of arterial blood sampling.

MATERIALS AND METHODS

Theory

Unlike glucose, [^{18}F]FDG is largely excreted by the kidneys without being resorbed by the renal proximal tubules and is continuously accumulated in the urinary bladder [25]. Let $C_W(t)$ be the radioactivity concentration of [^{18}F]FDG in whole-blood, k_F be the glomerular filtration rate of kidney, $f_u(t)$ be the time-varying urine flow, and $Q_B(t)$ be the total accumulated activity of [^{18}F]FDG at time t in the urinary bladder of volume $V_B(t)$. Figure 1 illustrates a simplified compartmental model configuration that describes the tracer kinetics in the renal system. Here, the renal tubules system of the kidney is modeled as a single-exponential dispersion kernel, $D(t)$, given by:

$$D(t)=\frac{1}{\tau}e^{-(t-\Delta)/\tau} \quad \text{Eq. 1}$$

where Δ and τ represent, respectively, the time shift and the dispersion for the blood to transit across the kidney. According to the model configuration of Figure 1, the radioactivity concentration of [^{18}F]FDG in urine at the outflow of kidney, C_u, is given by:

$$C_u(t)=k_F D(t) \otimes C_W(t) \quad \text{Eq. 2}$$

where $\otimes$ denotes convolution integration. To simplify the renal modeling procedure and to improve parameter identifiability, it is assumed that the urine flow (f_u) associated with the accumulation of [^{18}F]FDG in the urinary bladder is proportional to the rate of change of bladder volume (dV_B/dt) and can be empirically modeled by a one-exponential function, i.e., $V_B(t) = A(1 - e^{-\omega t})$ and $dV_B/dt = f_u(t) = A\omega e^{-\omega t}$, where A and ω are determined by fitting V_B to the bladder volume measurements. The following inhomogeneous linear differential equation can be derived for $Q_B(t)$:

$$\frac{d}{dt}Q_B(t)=f_u(t)C_u(t) \quad \text{Eq. 3}$$

With an intravenous tracer administration, the tracer kinetics observed in blood can generally be described by sum-of-exponentials models [26] and the [^{18}F]FDG clearance in whole-blood can be assumed to follow a one-exponential function at late times:

$$C_W(t)=C_W(t_m)e^{\lambda(t_m-t)} \quad \text{Eq. 4}$$

where λ (min^{-1}) represents the clearance rate of [^{18}F]FDG in whole-blood at late times and ($C_W(t_m)$ represents the whole-blood radioactivity concentration measured at the end of the experiment (at time t_m). Inserting Eq. 2 and Eq. 4 into Eq. 3 and integrating from t_i to t_{i+1} yields:

$$Q_B(t_{i+1})-Q_B(t_i)=k_F C_W(t_m)\int_{t_i}^{t_{i+1}} f_u(t)D(t)\otimes e^{\lambda(t_m-t)}dt \quad \text{Eq. 5}$$

Since multiple PET frames are available at late times (t > 35 min), improved parameter estimation is expected by minimizing the following cost function with $Q_B(t)$ measured at multiple late-time intervals [t_i, t_{i+1}]:

$$\min\left\{\sum_i \left\| Q_B(t_{i+1})-Q_B(t_i)-k_F C_W(t_m)\int_{t_i}^{t_{i+1}} f_u(t)D(t)\otimes e^{\lambda(t_m-t)}dt \right\|^2\right\} \quad \text{Eq. 6}$$

and the whole-blood sample measurements at late times (e.g., t_i > 35 min) can be estimated by Eq. 4 once λ is determined.

Animal Preparations and Experimental Procedures

All animal experiments were performed in accordance with institutional guidelines and a protocol approved by the Animal Research Committee of the University of California, Los Angeles. Nine male C57BL/6 mice (6 nonfasting and 3 fasting; 26.6 ± 4.9 g) were studied. Details of the experimental procedures have been reported in previous studies [21, 24, 27]. In brief, the animals were anesthetized with inhalant anesthesia (1.5%–2% isoflurane in 100% oxygen) and the body temperature of the mice was maintained at 37 °C by a thermostatically-controlled heating pad. The left femoral artery was cannulated with a surgically inserted polyethylene catheter (PE10; Intramedic, Clay-Adams). Small-animal PET was performed in list-mode on a microPET Focus 220 scanner (Concorde Microsystems, LLC), immediately after a bolus of [^{18}F]FDG (20.9 ± 5.7 MBq; 50–60 μL) was administered. Serial blood samples were collected manually at the femoral catheter and were subsequently pipetted to preweighed test tubes, weighed, and counted in a gamma counter (WIZARD 3"; PerkinElmer Life Sciences). After the PET scan was completed, a 10-min CT scan was acquired with a small-animal CT scanner (MicroCAT II; ImTek Inc.). The list-mode PET data were binned to a framing protocol of 1×3 s, 10×0.5 s, 1×2 s, 1×4 s, 6×5 s, 1×10 s, 2×30 s, 2×120 s, 1×180 s, 2×600 s, and 2×900 s (for 60-min scan) or 3×900 s (for 90-min scan). After correction for radioactive decay, random coincidences, and dead-time losses, the PET data were reconstructed using Fourier rebinning and a two-dimensional filtered backprojection algorithm with a ramp filter cut off at the Nyquist frequency and a zoom factor of 4.74, resulting in a voxel size of 0.4×0.4×0.8 mm^3. The small-animal CT images were coregistered with PET data for attenuation correction [28].

[^{18}F]FDG Kinetic Model

The standard three-compartment [^{18}F]FDG model [2] was used to fit the liver and muscle TACs. The state equations for the kinetics of [^{18}F]FDG in tissue are given by:

$$\frac{d}{dt}C_E(t)=K_1C_P(t)-(k_2+k_3)C_E(t)+k_4C_M(t)\ \frac{d}{dt}C_M(t)=k_3C_E(t)-k_4C_M(t) \quad \text{Eq. 7}$$

where $C_E(t)$ and $C_M(t)$ represent free and phosphorylated forms of [^{18}F]FDG in extravascular space of tissue, respectively; $C_P(t)$ represents arterial plasma IF; K_1 (mL/min/g) and k_2 (min^{-1}) are the forward and reverse transport constants of [^{18}F]FDG between tissue and plasma; and k_3 (min^{-1}) and k_4 (min^{-1}) are the phosphorylation and dephosphorylation rate constants in tissue. A time-dependent plasma-to-whole-blood [^{18}F]FDG equilibrium ratio, $R_{PB}(t)$, previously calculated at our laboratory [9] was used to account for the differences between [^{18}F]FDG concentrations in plasma and whole-blood:

$$R_{PB}(t)=0.386e^{-0.191t}+1.165. \quad \text{Eq. 8}$$

The model-predicted radioactivity concentration in tissue, $C_T(t)$, is given by:

$$C_T(t)=C_E(t)+C_M(t)+v_b\left(\frac{C_P(t)}{R_{PB}(t)}\right) \quad \text{Eq. 9}$$

where v_b (mL/g) represents the blood volume in tissue. The [^{18}F]FDG uptake constant (K_i) can be calculated from the kinetic constant estimates [1, 2]:

$$\mathrm{K_i}=\frac{K_1k_3}{k_2+k_3} \quad \text{Eq. 10}$$

which can also be determined by the Patlak graphical analysis [3].

Plasma Input Function

Standard kinetic modeling in PET assumes that the complete time course of plasma IF is available so that the kinetic constant parameters can be estimated by fitting the compartment model to the measured tissue TACs [4]. In contrast, the SIME approach [18, 19] assumes that (i) the plasma IF is unknown (or partially known) and can be parameterized by a mathematical model/equation and (ii) multiple tissue TACs of distinct kinetics are driven by the same IF. In this study, the parametric IF model was described by a sum of 4-exponential functions [29]:

$$C_P(t)=A_1e^{-\beta_1t}+A_2e^{-\beta_2t}+A_3e^{-\beta_3t}-(A_1+A_2+A_3)e^{-\beta_4t} \quad \text{Eq. 11}$$

where $A_1 - A_3$ (Bq/mL) and $\beta_1 - \beta_4$ (min^{-1}) can be determined by nonlinear least-squares fitting. Thus the input function estimated by the proposed hybrid approach (IF_{HYBRID}) consists of two steps: the late-time blood samples are first derived by the renal modeling technique (Eq. 4 and Eq. 6); the kinetic constants in the tissue TACs and the parameters that described the *estimated* plasma IF are determined by simultaneously fitting the [^{18}F]FDG model (Eq. 7 and Eq. 9) to the liver and muscle TACs and the parametric IF model (Eq. 11) to the plasma curve constructed by joining the early-time LV data ($t \leq 1$ min) corrected for partial-volume, delay and dispersion [24], and erythrocyte uptake (Eq. 8) and the late-time blood data ($t > 35$ min) derived in the first step, while blood data between 1-min and 35-min postinjection that were supposed to be unavailable were interpolated by the parametric IF model (Eq. 11). The "gold standard" input function (IF_{GS}) for each study, with which the

estimated IF was compared, was constructed in the same way but with all serial blood samples taken after 1-min postinjection.

Data Analysis

Results are presented as mean ± standard deviation (SD) unless otherwise stated. Statistical analyses were performed using Prism 4.03 (GraphPad Software, Inc.). A *P*-value of less than 0.05 was considered statistically significant.

Both PET image data and blood data were converted to absolute radioactivity concentration (Bq/mL) with the cross-calibration factor derived from routine cylinder phantom experiments. Images were analyzed using AMIDE (http://amide.sourceforge.net/). Three-dimensional ellipsoid volumes of interest (VOIs) were manually drawn over the brain, myocardium, skeletal muscle of forelegs, liver, and kidney on the coregistered PET/CT images, which provided anatomic references for VOI placement. The VOIs were applied to each time frame of the PET images, and the average radioactivity concentration was computed to obtain the corresponding TACs. Because uptake in the tissues was relatively homogeneous within the VOIs and the background radioactivity was low, background subtraction and partial-volume correction were not performed.

Derivation of the complete time course of the plasma IF can be improved with the TAC obtained from the LV. Spherical VOI of 1.5 mm in diameter was drawn on the PET image in the region that corresponded to the LV, which could be visualized during the first 10 s postinjection. Due to continuous excretion of [^{18}F]FDG by the kidneys, the volume of [^{18}F]FDG in the urinary bladder increases as a function of time. The PET data were scaled with an empirical threshold value of about 65–75% of the global maximum, which was found to provide good boundary delineation of bladder VOIs on the fused PET/CT image [30], and VOIs that covered the entire bladder were drawn frame-by-frame and the total accumulated activity curve of the urinary bladder was then calculated.

The best estimates of [^{18}F]FDG clearance rate in plasma and delay and dispersion of blood across the kidney and accumulation of ^{18}F-activity in urinary bladder were determined by minimizing the cost function given by Eq. 6. Simultaneous fitting of [^{18}F]FDG model (Eq. 7 and Eq. 9) and parametric IF (Eq. 11) to the experimental data was performed using SAAM II [31]. The accuracy of the input function obtained without using the renal modeling technique was also evaluated using the last blood sample collected at the end of PET imaging, i.e., only the second step of the proposed method was applied to estimate the IF ($IF_{1\text{-}BS}$). Under the assumption that [^{18}F]FDG is rapidly cleared from the liver [25], the image-derived liver TAC (IF_{LIVER}) has been suggested as an alternative plasma IF [14, 32] and was also investigated in this study.

Areas under the curve (AUCs) were calculated for IF_{HYBRID} (AUC_{HYBRID}), $IF_{1\text{-}BS}$ ($AUC_{1\text{-}BS}$), and IF_{LIVER} (AUC_{LIVER}). Their correspondences with those calculated using IF_{GS} (AUC_{GS}) were assessed by means of linear regression. The [^{18}F]FDG uptake constant (K_i) values in the brain, myocardium, skeletal muscle, and liver were estimated by the Patlak graphical analysis [3] using various IFs and tissue data from 15–60 min [24]. Limits of agreement of AUC and Patlak K_i estimates obtained by different methods and those by IF_{GS} were assessed by the Bland-Altman analysis [33], where the differences between measurements on the same animal by two methods were plotted against the average, and the estimated bias and its 95% confidence interval (CI) were computed. The Friedman's test followed by Dunn's multiple comparison test [34] was used to assess whether the AUCs and Patlak K_i obtained by various approaches were statistically different from those obtained by IF_{GS}.

RESULTS

Radioactivity and Urine Volume in Urinary Bladder

Figure 2 shows typical total accumulated radioactivity and the volume in urinary bladder as a function of time obtained in three mice. It can be seen that the increase in volume was not linear and that the accumulation of [^{18}F]FDG in the urinary bladder varied differently among different animals. Table 1 summarizes estimates of various parameters, including the clearance rate of [^{18}F]FDG in whole-blood at late time (λ), dispersion (τ) and delay (Δ) time constants for accumulating ^{18}F-activity to the urinary bladder in the form of urine. The average dispersion and delay time constants were 1.89 ± 0.98 min and 2.13 ± 0.85 min, respectively, and the parameter estimates were reasonably consistent among different animals. In spite of the nonlinear increase in bladder volume and difference in accumulation rate of [^{18}F]FDG in the urinary bladder, the proposed renal modeling technique was able to provide the blood clearance estimate comparable to that estimated using multiple late-time blood samples (0.0212 ± 0.0106 min^{-1} vs. 0.0177 ± 0.0063 min^{-1}, Wilcoxon signed rank test, $P = 0.425$).

Estimation of Input Function

Figure 3 shows plasma IFs and their estimation by various approaches in all studies. The partial-volume-, delay-, dispersion-, and R_{PB}-adjusted early-time LV TAC was used to represent the plasma data within 1-min postinjection, and the late-time plasma data were corrected for the uptake by erythrocytes. The estimated IF_{HYBRID} closely resembled IF_{GS} that required arterial cannulation and continuous blood sampling. The mean absolute differences between IF_{HYBRID} and IF_{GS} were 8.3% ± 7.0% and 4.5% ± 2.7% at 30- and 60-min, respectively. However, the image-derived liver TAC (IF_{LIVER}) deviated substantially from IF_{GS}.

The AUC of the estimated IF_{HYBRID}, $IF_{1\text{-}BS}$, and IF_{LIVER} was compared with that of the IF_{GS}, which was calculated by fitting the [^{18}F]FDG model with all available blood sample data. The correspondences and the limits of agreement between AUC_{GS} and AUC_{HYBRID}, $AUC_{1\text{-}BS}$, and AUC_{LIVER} are shown in Figure 4. Although none of the regression lines was significantly different from the line of identity (extra sum-of-squares F-test, $P > 0.05$), the slope of the regression line between AUC_{LIVER} and AUC_{GS} tended to differ from one ($P = 0.066$). There were no significant differences between the AUC values of plasma IFs obtained by different methods when compared with AUC_{GS} (Dunn's multiple comparison test, $P > 0.05$). The mean biases from AUC_{GS} were similar for AUC_{HYBRID} and $AUC_{1\text{-}BS}$ (1.82 vs. 2.31 MBq/mL×min), but the 95% limits of agreement (mean ± 1.96 SD) with AUC_{GS} were better for AUC_{HYBRID} (95% CI: −4.37–8.01 MBq/mL×min) than for $AUC_{1\text{-}BS}$ (95% CI: −9.80–14.42 MBq/mL×min). In contrast, the mean bias (−4.70 MBq/mL×min) and the 95% CI (−22.08–12.67 MBq/mL×min) for the difference between AUC_{LIVER} and AUC_{GS} were found to be much larger.

[^{18}F]FDG Uptake Constant

Figure 5 shows the comparison of K_i calculated for the brain, myocardium, skeletal muscle, and liver using Patlak analysis with IF_{HYBRID} and IF_{GS}. The slopes of the regression lines were close to 1 and the intercepts were nearly equal to 0, with the Spearman correlation coefficients of 0.983, 0.983, 1.0, and 0.933 for the brain, myocardium, skeletal muscle, and liver, respectively. The limits of agreement between Patlak K_i estimates were further examined by the Bland-Altman analysis and are shown in Figure 6. The Bland-Altman plots show a slight bias in K_i estimated with IF_{HYBRID} (−0.00094, −0.0044, −0.00029, and −0.0001 mL/min/g in brain, myocardium, muscle, and liver, respectively) and $IF_{1\text{-}BS}$ (−0.00095, −0.0024, −0.00022, and −0.00027 mL/min/g in brain, myocardium, muscle, and

liver, respectively) in comparison with K_i estimated using IF_{GS}. A little wider spread of K_i values for $IF_{1\text{-}BS}$ compared with IF_{HYBRID} was observed, and the differences and discrepancies were much more prominent for IF_{LIVER}. Table 2 shows the mean ratios of Patlak K_i values in various tissues determined with IF_{HYBRID}, $IF_{1\text{-}BS}$ and IF_{LIVER} to those obtained with IF_{GS}. The K_i ratios for IF_{HYBRID} and $IF_{1\text{-}BS}$ were close to 1. However, for IF_{LIVER}, the K_i ratios in brain and skeletal muscle ranged from −0.28 to 1.02 and from −0.21 to 1.04, respectively, and differed significantly from 1 ($P < 0.05$). The negative K_i ratios were caused by two different cases in which the use of liver as IF produced negative K_i estimates for the brain and skeletal muscle, respectively.

DISCUSSION

Accurate quantification of dynamic PET data is directly related to the precise definition of the IF, which is usually obtained via arterial catheterization and continuous blood sampling. The invasiveness of aseptic microsurgery, the small size of rodents and the limitation in total blood volume pose considerable technical complexities and methodological challenges to acquiring IF measurements without causing much distress and disturbance to the animals. Our results show that the proposed hybrid method is able to estimate the IF reliably and to provide good AUC and K_i estimates when compared to those obtained with the gold standard IF, which requires serial blood sampling.

The ideal situation would be if blood sampling could be eliminated completely. However, a number of studies have demonstrated that at least one blood sample is needed for scaling the estimated IF and significantly more accurate IF estimation is achieved with increasing number of blood sample measurements [18–20, 22, 23]. Consistent with the findings of those studies, the use of one blood sample in the estimation process provided much better estimated IF than without using any blood sample (data not shown). On the contrary, the main advance of this study is that the late-time blood measurements are estimated by making use of the relationship between plasma clearance and total accumulated radioactivity in bladder [24] and the excretion pathway of [^{18}F]FDG [25] instead of collecting multiple blood samples to improve the accuracy of the estimated IF as in many previous studies.

The proposed renal model is certainly a simplified physio-anatomical model for the complex and heterogeneous structure of kidney. Nonetheless, the estimated plasma clearance rate at late-time using the renal model is in line with the published data [21–23], whereas the mean tracer appearance time in the urinary bladder was found to be about 2–3 minutes and is in good agreement with previously reported values [24], thus indicating that useful information can be extracted from the proposed model. Further studies are clearly required to formulate a more representative compartmental model configuration that is able to resolve and describe different functional compartments of kidney under the limited spatial resolution of small-animal PET and to deal with renal failure condition (e.g., diabetes mellitus) when the kidneys could not excrete [^{18}F]FDG into the urine completely.

A more accurate approach to determine the total radioactivity and the capacity of the bladder would be to collect urine samples at timed intervals through urethral catheterization. However, the procedure is impractical in mice due to various anatomical, physiological, and technical considerations, including the gender of the animal, the size and material of the catheter, the disease condition, and the potential contamination of the urine specimens. Therefore, a completely noninvasive image-based approach is sought in this study. The total radioactivity and the volume of urinary bladder were calculated from the small-animal PET images with the aid of the threshold value determined using the fused PET/CT image. Potential errors in their calculations are mainly attributed to the spillover of the radioactivity from the surrounding tissues which is comparable to the radioactivity in the bladder at early

times. However, the effect of spillover of radioactivity from the surrounding tissues can be assumed to be small and negligible at late-time because the size of bladder VOI is usually much bigger than the spatial resolution, which is 1.7 mm full-width at half-maximum with the selected reconstruction settings, and the measured radioactivity is dominated by that in the urinary bladder. The bladder volume (~0.1–0.3 mL) determined at late-time is well within the published maximum observed in generic laboratory mice (0.5 mL; [35]), the value of which depends also on a number of factors, including the strain, gender and size of the mice, the study condition, the time of measurement, and the measurement technique being used. Therefore, the bladder capacity determined from the fused PET/CT image at late-time is expected to be close to the "actual" value, which was, however, not measured for each mouse because the urinary bladder was not harvested at the end of the experiment as the animal would micturate soon after euthanasia, resulting in erroneous urine volume determination and total ^{18}F-activity measurement.

Different from many other organs or tissues, which are supplied solely by arterial blood, the liver has dual blood supply from the hepatic artery and the portal vein. The use of dual blood supply in fitting [^{18}F]FDG kinetics of liver has been shown to provide more physiological reasonable estimates than the use of single blood supply [36, 37]. However, surgical cannulation of both hepatic artery and portal vein for blood sampling in rodents is not a trivial task and will only make the small-animal imaging procedure more complicated. Therefore, we used the arterial input to approximate the dual input to the liver and this is not expected to hamper the estimation capability of the proposed method.

Assuming the liver has relatively large blood volume and rapid [^{18}F]FDG clearance [25], the image-derived liver TAC has been suggested as a possible input function for small-animal [^{18}F]FDG PET studies [14, 32]. So far, however, no results have been published regarding the errors and the bounds of applicability of using this "reference tissue" as input function for quantitative analysis of [^{18}F]FDG PET data. It should be noted that [^{18}F]FDG uptake in liver is dependent upon the physiological status and metabolic conditions (e.g., fasting or hyperinsulinemia) of the animal. Our results show that Patlak K_i estimates derived using liver TAC as input function had large differences when compared to those obtained with the gold standard input function (Table 2 and Figure 6), despite the good correlations in AUCs between liver and plasma TACs (Figure 4e). The discrepancies are likely caused by the differences in the shape of liver and plasma TACs (Figure 3).

As [^{18}F]FDG does not cross murine erythrocyte membrane freely [38], the plasma-towhole blood activity concentration ratio will not reach relatively constant (i.e., equilibrium) until after ~25 min postinjection [9, 24]. Therefore, when a late-time whole-blood sample is available, the "equivalent" plasma radioactivity concentration can be obtained by adjusting the whole-blood radioactivity concentration with the equilibrium ratio. Because the arterial and venous blood concentrations are usually very similar at late-time and only one blood sample taken at the end of the experiment is needed for the proposed method, it is possible to replace the arterial blood sample by arterialized-venous or venous blood sample, which is easy to collect at the lateral caudal vein. This could further simplify the proposed procedure and make it useful in repeated/longitudinal dynamic [^{18}F]FDG PET studies on the same animal, where invasive blood sampling is infeasible.

It is anticipated that the accuracy and robustness of the proposed method can be further improved. For example, the threshold value for bladder boundary detection on the PET image can be determined using a calibrated phantom similar in shape and size to the bladder. Also, the procedure of defining bladder VOI on multiple image frames which is performed manually can be streamlined by some automatic VOI delineation algorithms so that the VOI defined will have less human intervention and higher reproducibility. Since the photon

attenuation was changed as the bladder got larger, the attenuation correction was only an approximation. Conceptually, this attenuation change can be accounted for, but the procedure is not expected to be simple and easy. As a result, the determination of total ^{18}F-activity and bladder volume at early times may be biased due to over-correction for photon attenuation using the attenuation map derived from the CT image acquired at late-time. Nonetheless, the renal modeling procedure depends only on the late-time measurements of total ^{18}F-activity and bladder volume, both of which are expected to be more accurate than their early-time measurements because of the more uniform distribution of ^{18}F-activity in the bladder volume at late times and the close approximation of photon attenuation resulting from a better alignment between CT and late-time PET images. As for modeling the time-varying urine flow, the one-exponential function is certainly an empirical choice. Other analytical functions (e.g., polynomials) may also be used for this purpose. To our knowledge, however, no data have yet been published to calculate urine flow rate in murine over a short time interval, probably because of the technical difficulties associated with frequent urine collection without increasing levels of pain and discomfort caused to the animal, and the urine flow (as well as the urine production rate) of 1 mL per day has been reported [39, 40]. Since the frequency of voiding and the void volume may change from time to time (e.g., the mouse may urinate more frequently during awake time when water intake is higher), the urine production rate is likely varying throughout the day. The nonlinear increase in the bladder volume curves indicates that the urine production rate is not constant over time and decreases as the bladder gets filled up. As for the computation and implementation aspects, the two-step estimation of the proposed hybrid approach can be reformulated into a one-step estimation procedure by unifying Eq. 4 and Eq. 11. Fitting an analytical function form for the IF is a common strategy to reduce statistical uncertainties in the measured blood data [41, 42]. In this study, a sum of 4-exponentials was used to describe the plasma IF characterized by the abrupt changes in radioactivity concentration immediately after tracer administration and to account for differences in injection schedule. An alternative approach is to use a physiological-based model to describe the tracer kinetics in blood/plasma. One such model has been proposed for human [^{18}F]FDG PET [29], but an optimal functional form has yet to be determined for rodents. We are currently exploring various approaches to address the issues as mentioned above.

CONCLUSIONS

In this study, we proposed and validated a hybrid approach that uses the total accumulated radioactivity in the urinary bladder and a blood sample collected at the end of the study as well as time-activity data from multiple tissues to estimate the plasma input function for dynamic mouse [^{18}F]FDG PET studies. By combining the proposed renal modeling technique with the simultaneous estimation, the estimated blood samples agreed well with those derived from the standard reference but invasive blood sampling approach. Importantly, this hybrid approach obviates the need of arterial catheterization as it requires only one late-time blood sample, which can be collected from the tail vein, thus making it possible to perform longitudinal dynamic [^{18}F]FDG PET studies on the same animal. Conversely, liver time-activity curve is unsuitable as an input function for absolute quantification of [^{18}F]FDG PET data, as it provides significantly biased estimates of uptake constant in various tissues.

Acknowledgments

This work was supported by National Institutes of Health (NIH) grants R01-EB001943 and P50-CA086306.

The authors would like to thank Waldemar Ladno, Judy Edwards, Antonia Luu, and David Stout for technical assistance in small-animal PET and CT imaging; Weber Shao, Dat Vu, and David Truong for computer and database support; and the UCLA Cyclotron staff for help with [^{18}F]FDG preparation.

REFERENCES

1. Sokoloff L, Reivich M, Kennedy C, et al. The [^{14}C]deoxyglucose method for the measurement of local cerebral glucose utilization: Theory, procedure and normal values in the conscious and anesthetized albino rat. J Neurochem. 1977; 28:897–916. [PubMed: 864466]
2. Huang S-C, Phelps ME, Hoffman EJ, Sideris K, Selin CJ, Kuhl DE. Noninvasive determination of local cerebral metabolic rate of glucose in man. Am J Physiol. 1980; 238:E69–E82. [PubMed: 6965568]
3. Patlak CS, Blasberg RG, Fenstermacher J. Graphical evaluation of blood-to-brain transfer constants from multiple-time uptake data. J Cereb Blood Flow Metab. 1983; 3:1–7. [PubMed: 6822610]
4. Huang, S-C.; Phelps, ME. Principles of tracer kinetic modeling in positron emission tomography and autoradiography. In: Phelps, ME.; Mazziotta, JC.; Schelbert, HR., editors. Positron Emission Tomography and Autoradiography: Principles and Applications for the Brain and Heart. New York: Raven Press; 1986. p. 287-346.
5. Ashworth, S.; Ranicar, A.; Bloomfield, PM.; Jones, T.; Lammertsma, AA. Development of an on-line blood detector system for PET studies in small animals. In: Myers, R.; Cunningham, V.; Bailey, D.; Jones, T., editors. Quantification of Brain Function Using PET. San Diego: Academic Press; 1996. p. 62-66.
6. Weber B, Burger C, Biro P, Buck A. A femoral arteriovenous shunt facilitates arterial whole blood sampling in animals. Eur J Nucl Med Mol Imaging. 2002; 29:319–323. [PubMed: 12002705]
7. Pain F, Lanièce P, Mastrippolito R, Gervais P, Hantraye P, Besret L. Arterial input function measurement without blood sampling using a β-microprobe in rats. J Nucl Med. 2004; 45:1577–1582. [PubMed: 15347727]
8. Laforest R, Sharp TL, Engelbach JA, et al. Measurement of input functions in rodents: challenges and solutions. Nucl Med Biol. 2005; 32:679–685. [PubMed: 16243642]
9. Wu H-M, Sui G, Lee C-C, et al. In vivo quantitation of glucose metabolism in mice using small-animal PET and a microfluidic device. J Nucl Med. 2007; 48:837–845. [PubMed: 17475972]
10. Eberl S, Anayat AR, Fulton RR, Hooper PK, Fulham MJ. Evaluation of two population-based input functions for quantitative neurological FDG PET studies. Eur J Nucl Med. 1997; 24:299–304. [PubMed: 9143468]
11. Meyer PT, Circiumaru V, Cardi CA, Thomas DH, Bal H, Acton PD. Simplified quantification of small animal [^{18}F]FDG PET studies using a standard arterial input function. Eur J Nucl Med Mol Imaging. 2006; 33:948–954. [PubMed: 16699768]
12. Gambhir SS, Schwaiger M, Huang S-C, et al. Simple noninvasive quantification method for measuring myocardial glucose utilization in humans employing positron emission tomography and fluorine-18 deoxyglucose. J Nucl Med. 1989; 30:359–366. [PubMed: 2786939]
13. Chen K, Bandy D, Reiman E, et al. Noninvasive quantification of the cerebral metabolic rate for glucose using positron emission tomography, ^{18}F-fluoro-2-deoxyglucose, the Patlak method, and an image-derived input function. J Cereb Blood Flow Metab. 1998; 18:716–723. [PubMed: 9663501]
14. Green LA, Gambhir SS, Srinivasan A, et al. Noninvasive methods for quantitating blood time-activity curves from mouse PET images obtained with fluorine-18-fluorodeoxyglucose. J Nucl Med. 1998; 39:729–734. [PubMed: 9544690]
15. Wu H-M, Huang S-C, Allada V, et al. Derivation of input function from FDG-PET studies in small hearts. J Nucl Med. 1996; 37:1717–1722. [PubMed: 8862318]
16. Wong K-P, Feng D, Meikle SR, Fulham MJ. Segmentation of dynamic PET data using cluster analysis. IEEE Trans Nucl Sci. 2002; 49:200–207.
17. Kim J, Herrero P, Sharp T, et al. Minimally invasive method of determining blood input function from PET images in rodents. J Nucl Med. 2006; 47:330–336. [PubMed: 16455640]
18. Feng D, Wong K-P, Wu C-M, Siu W-C. A technique for extracting physiological parameters and the required input function simultaneously from PET image measurements: Theory and simulation study. IEEE Trans Inform Technol Biomed. 1997; 1:243–254.
19. Wong K-P, Feng D, Meikle SR, Fulham MJ. Simultaneous estimation of physiological parameters and the input function-*In vivo* PET data. IEEE Trans Inform Technol Biomed. 2001; 5:67–76.

20. Riabkov DY, Di Bella EVR. Estimation of kinetic parameters without input functions: Analysis of three methods for multichannel blind identification. IEEE Trans Biomed Eng. 2002; 49:1318–1327. [PubMed: 12450362]
21. Ferl GZ, Zhang X, Wu H-M, Huang S-C. Estimation of the ^{18}F-FDG input function in mice by use of dynamic small-animal PET and minimal blood sample data. J Nucl Med. 2007; 48:2037–2045. [PubMed: 18006615]
22. Fang Y-H, Muzic RF Jr. Spillover and partial-volume correction for image-derived input functions for small-animal ^{18}F-FDG PET studies. J Nucl Med. 2008; 48:606–614. [PubMed: 18344438]
23. Su Y, Shoghi KI. Single-input-dual-output modeling of image-based input function estimation. Mol Imaging Biol. 2009; 12:286–294. [PubMed: 19949986]
24. Wong K-P, Sha W, Zhang X, Huang S-C. Effects of administration route, dietary condition, and blood glucose level on kinetics and uptake of ^{18}F-FDG in mice. J Nucl Med. 2011; 52:800–807. [PubMed: 21498533]
25. Gallagher BM, Fowler JS, Guterson NI, MacGregor RR, Wan CN, Wolf AP. Metabolic trapping as a principle of radiopharmaceutical design: some factors responsible for the biodistribution of [^{18}F]2-deoxy-2-fluoro-D-glucose. J Nucl Med. 1978; 19:1154–1161. [PubMed: 214528]
26. Jacquez, JA. Compartmental Analysis in Biology and Medicine. 2nd ed.. Ann Arbor: The University of Michigan Press; 1985.
27. Huang, SC.; Wu, HM.; Truong, D., et al. A public domain dynamic mouse FDG microPET image data set for evaluation and validation of input function derivation methods. IEEE Medical Imaging Conference; San Diego, California. 2006. p. 2681-2683.
28. Chow PL, Rannou FR, Chatziioannou AF. Attenuation correction for small animal PET tomographs. Phys Med Biol. 2005; 50:1837–1850. [PubMed: 15815099]
29. Feng D, Huang S-C, Wang X. Models for computer simulation studies of input functions for tracer kinetic modeling with positron emission tomography. Int J Biomed Comput. 1993; 32:95–110. [PubMed: 8449593]
30. Wong, K-P.; Huang, S-C. Modeling approach to estimate [^{18}F]FDG blood sample measurements in mice by use of urinary bladder time-activity data. IEEE Medical Imaging Conference; Dresden, Germany. 2008. p. 5572-5576.
31. Barrett PH, Bell BM, Cobelli C, et al. SAAM II: Simulation, analysis, and modeling software for tracer and pharmacokinetic studies. Metabolism. 1998; 47:484–492. [PubMed: 9550550]
32. Yu AS, Lin H-D, Huang S-C, Phelps ME, Wu H-M. Quantification of cerebral glucose metabolic rate in mice using ^{18}F-FDG and small-animal PET. J Nucl Med. 2009; 50:966–973. [PubMed: 19443595]
33. Bland JM, Altman DG. Statistical methods for assessing agreement between two methods of clinical measurement. Lancet. 1986; i:307–310. [PubMed: 2868172]
34. Daniel, WW. Applied Nonparametric Statistics. 2nd ed.. Duxbury Press; 2000.
35. Quimby, FW.; Luong, RH. Clinical chemistry of the laboratory mouse. In: Fox, JG.; Barthold, SW.; Davisson, MT.; Newcomer, CE.; Quimby, FW., editors. The Mouse in Biomedical Research: Normative Biology, Husbandry, and Models. New York: Academic Press; 2007. p. 171-216.
36. Munk OL, Bass L, Roelsgaard K, Bender D, Hansen SB, Keiding S. Liver kinetics of glucose analogs measured in pigs by PET: Importance of dual-input blood sampling. J Nucl Med. 2001; 42:795–801. [PubMed: 11337579]
37. Brix G, Ziegler SI, Bellemann ME, et al. Quantification of [^{18}F]FDG uptake in the normal liver using dynamic PET: Impact and modeling of the dual hepatic blood supply. J Nucl Med. 2001; 42:1265–1273. [PubMed: 11483690]
38. Buxton DB. Glucose permeability in nonprimate erythrocytes. J Nucl Med. 1999; 40:2125–2126. [PubMed: 10616896]
39. Clark B, Smith DA. Pharmacokinetics and toxicity testing. Crit Rev Toxicol. 1984; 12:343–385. [PubMed: 6378530]
40. Hoyt, RF., Jr; Hawkins, JV.; St Clair, MB.; Kennett, MJ. Mouse physiology. In: Fox, JG.; Barthold, SW.; Davisson, MT.; Newcomer, CE.; Quimby, FW., editors. The Mouse in Biomedical Research: Normative Biology, Husbandry, and Models. New York: Academic Press; 2007. p. 23-90.

41. Wong, K-P.; Huang, S-C.; Fulham, MJ. Evaluation of an input function model that incorporates the injection schedule in FDG-PET studies. IEEE Medical Imaging Conference; San Diego, California. 2006. p. 2086-2090.

42. Chen K, Huang S-C, Yu DC. The effects of measurement errors in plasma radioactivity curve on parameter estimation in positron emission tomography. Phys Med Biol. 1993; 36:1183–1200. [PubMed: 1946602]

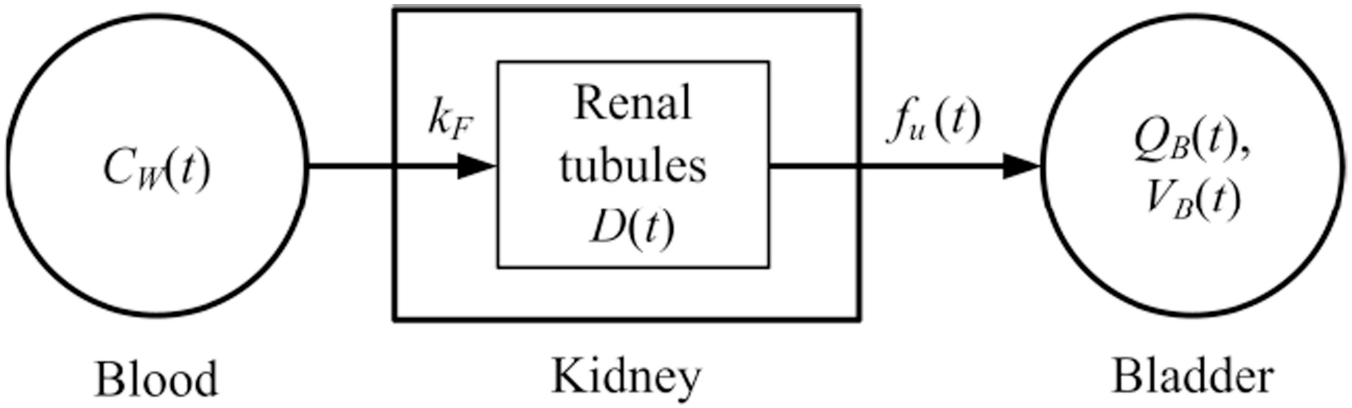

Figure 1.
A simplified compartmental model for [^{18}F]FDG excretion in the renal system.

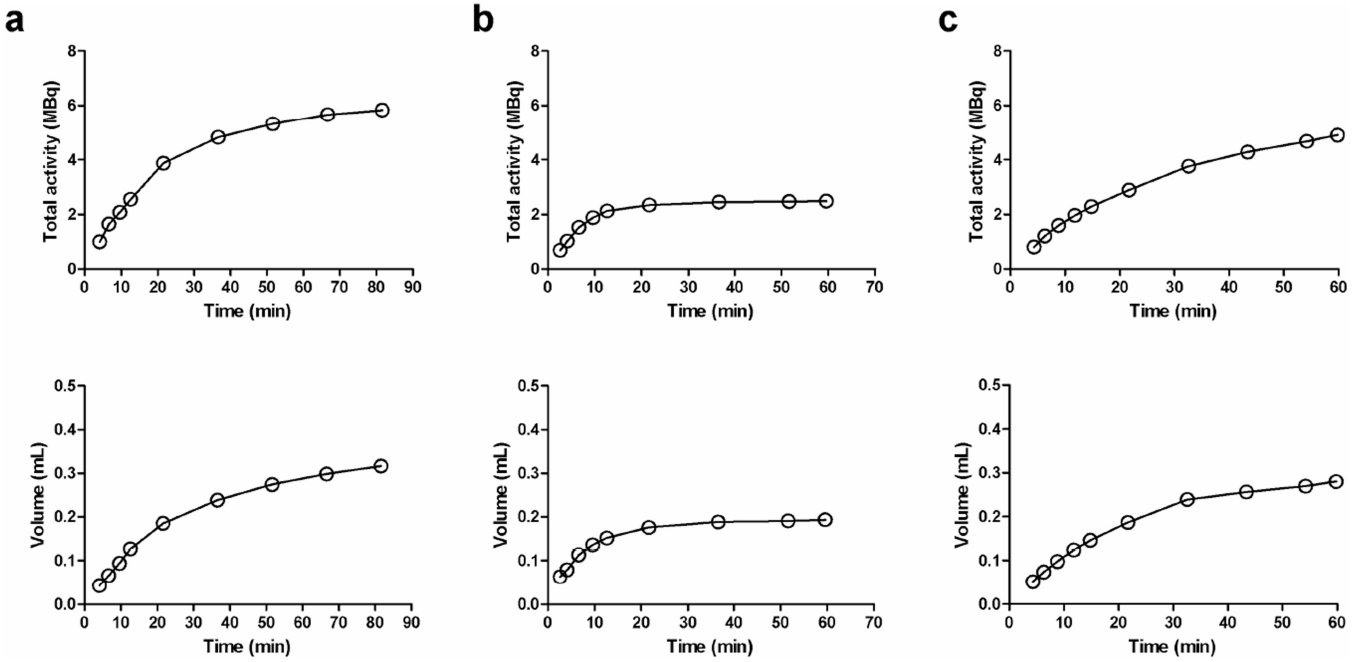

Figure 2.
Representative total accumulated radioactivity (top row) and the corresponding volume (bottom row) of ^{18}F-activity in urinary bladder measured in three mice.

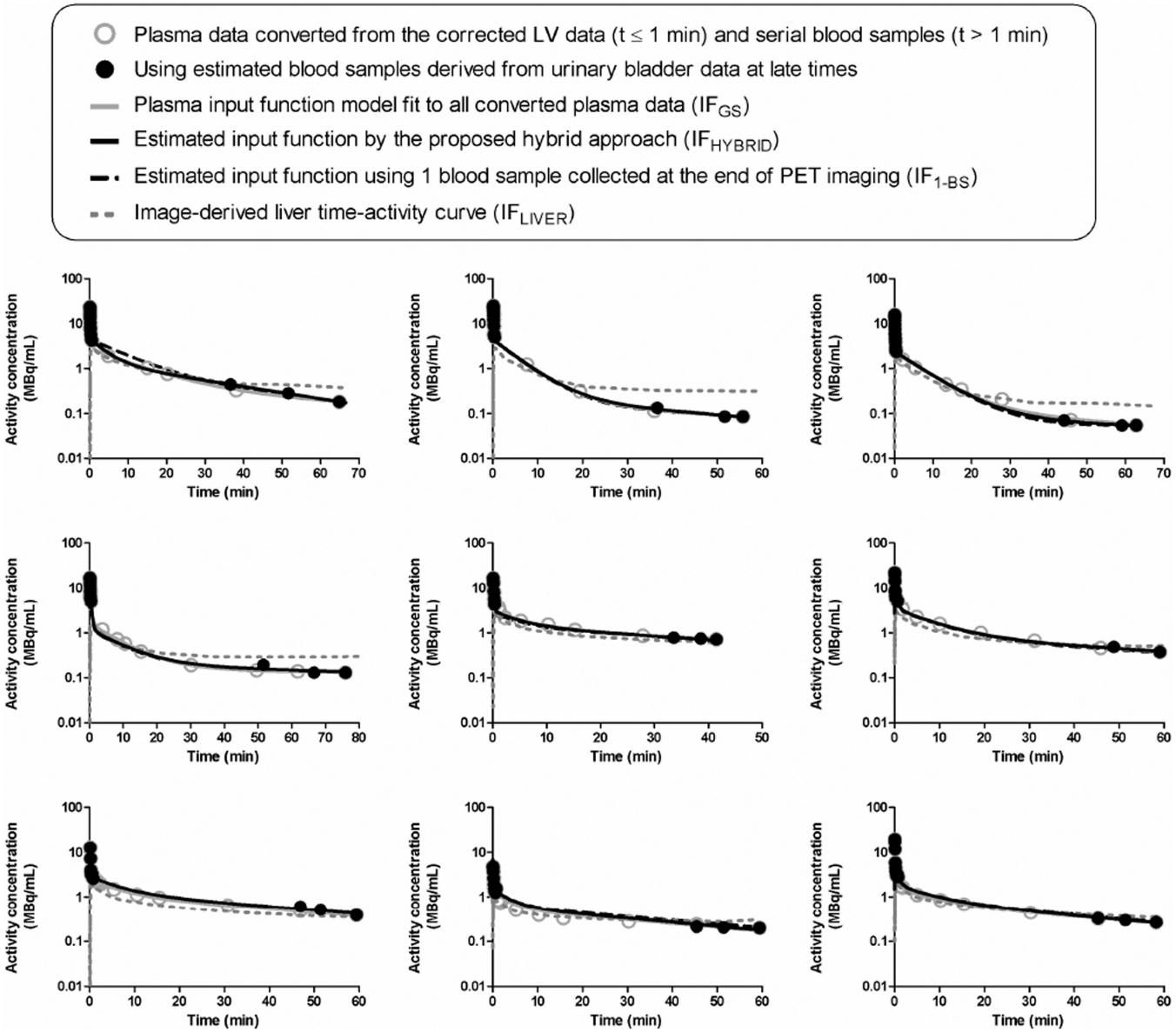

Figure 3.
Comparison of input functions obtained in all animals using different methods.

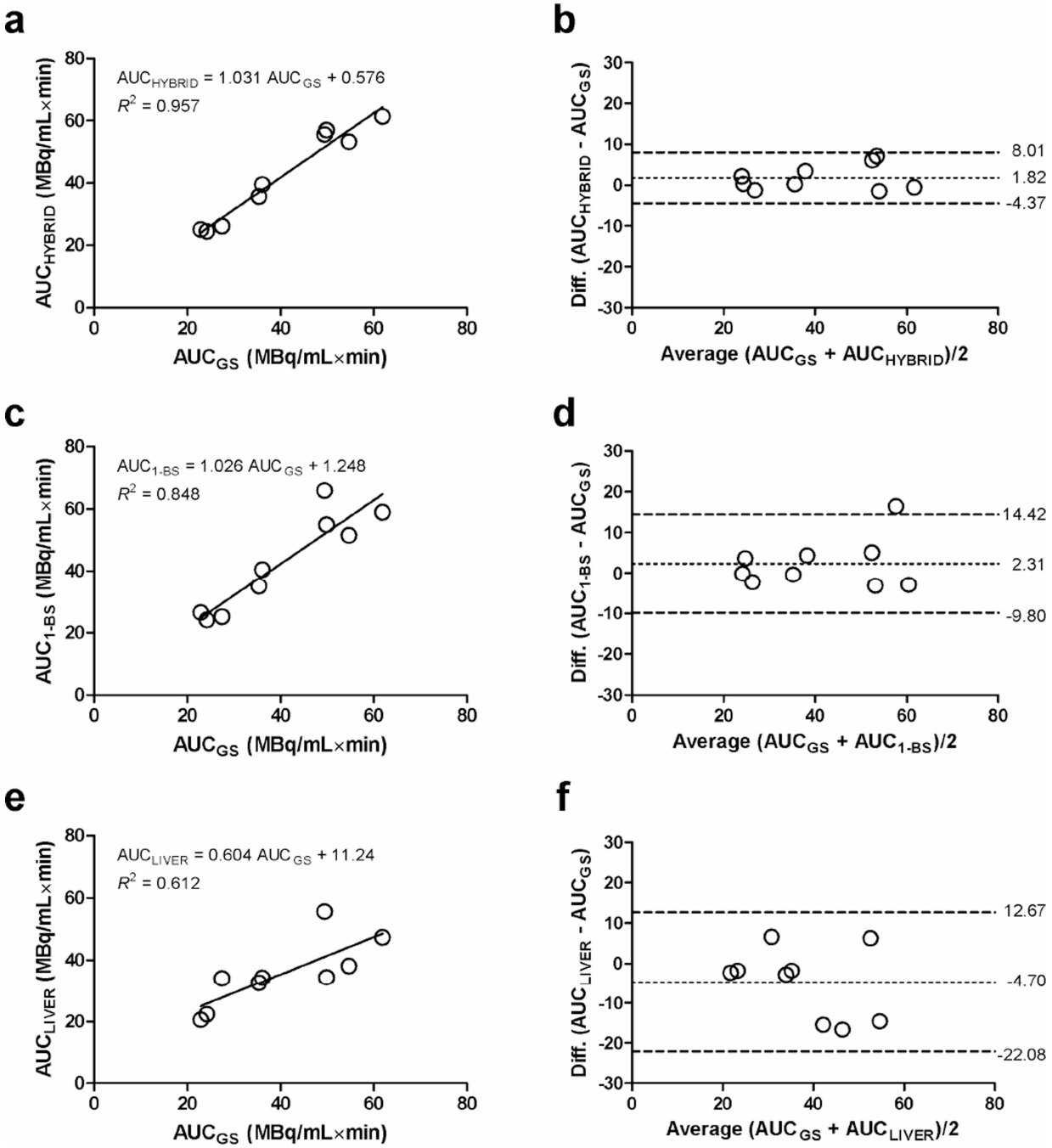

Figure 4.

Graphs show the linear regression between AUC_{GS} and (a) AUC_{HYBRID}, (c) $AUC_{1\text{-}BS}$, and (e) AUC_{LIVER}. The limits of agreement between AUC_{GS} and AUC_{HYBRID}, $AUC_{1\text{-}BS}$, and AUC_{LIVER} are shown in subpanels (b), (d), and (f), in which the dotted line represents the mean difference in AUC, and the dashed lines represent the 95% confidence interval for the difference (mean ± 1.96 SD).

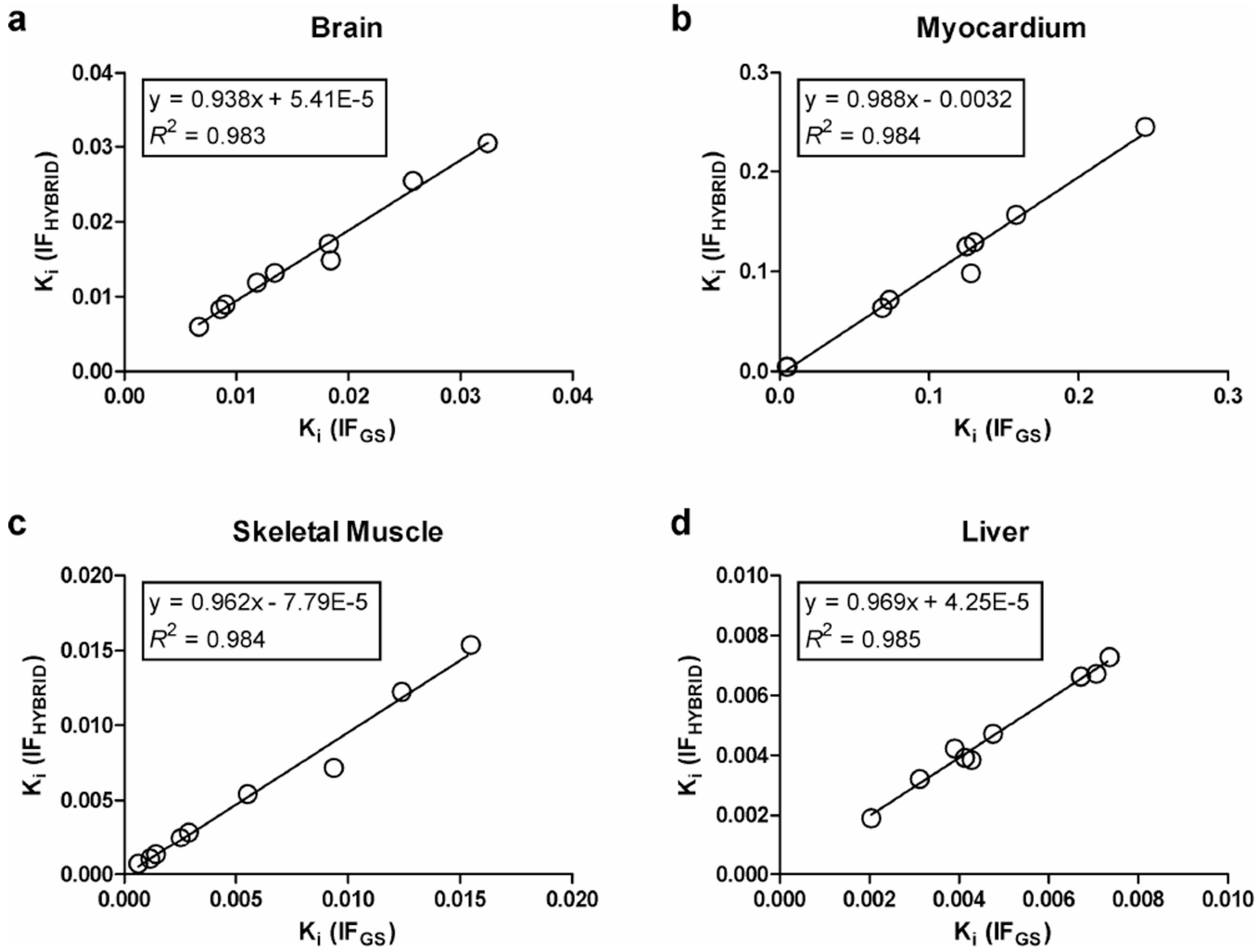

Figure 5.

Comparison of Patlak K_i in (a) brain, (b) myocardium, (c) skeletal muscle, and (d) liver, determined with IF_{HYBRID} and IF_{GS}.

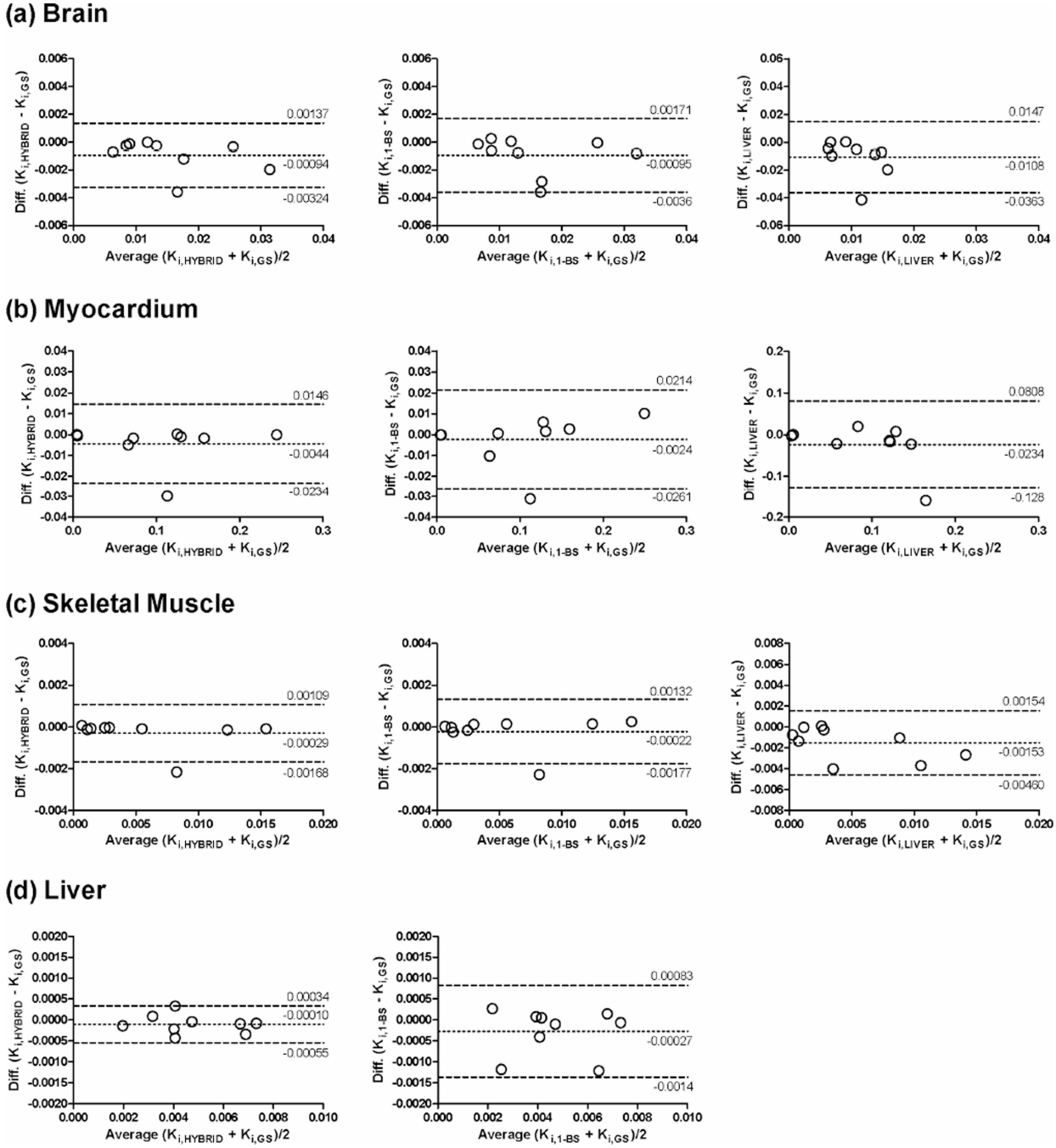

Figure 6.

Limits of agreement between Patlak K_i obtained for (a) brain, (b), myocardium, (c) skeletal muscle, and (d) liver, using IF_{GS} ($K_{i,GS}$), IF_{HYBRID} ($K_{i,HYBRID}$, left column), $IF_{1\text{-}BS}$ ($K_{i,1\text{-}BS}$, middle column), and IF_{LIVER} ($K_{i,LIVER}$, right column). Dotted line represents the mean difference in K_i; dashed lines represent the 95% confidence interval for the difference (mean ± 1.96 SD). Note the different ranges for the ordinate axis when liver TAC was used as the input function (right column).

Table 1

Estimated [^{18}F]FDG clearance rate in blood ($\hat{\lambda}$), dispersion (τ) and delay (Δ) time constants for filtrating blood in the kidney and accumulating ^{18}F-activity to the urinary bladder.

	Parameter estimates		
Mouse	**λ (min^{-1})**	**τ (min)**	**Δ (min)**
1	0.0294	0.91	2.91
2	0.0300	1.00	1.61
3	0.0173	1.82	1.99
4	0.0258	1.80	3.19
5	0.0092	2.07	1.81
6	0.0247	1.82	0.37
7	0.0361	1.28	2.83
8	0.0040	4.26	2.23
9	0.0144	2.05	2.21
Mean	0.0212	1.89	2.13
SD	0.0106	0.98	0.85

Table 2

Mean ratios of Patlak K_i estimate in various regions determined with IF_{HYBRID}, $IF_{1\text{-}BS}$, IF_{LIVER} and the gold standard IF (IF_{GS}).

	Region			
Input function	**Brain**	**Myocardium**	**Muscle**	**Liver**
IF_{HYBRID}	0.94 ± 0.06	0.95 ± 0.08	0.96 ± 0.09	0.98 ± 0.05
$IF_{1\text{-}BS}$	0.95 ± 0.08	0.96 ± 0.10	0.96 ± 0.10	0.95 ± 0.15
IF_{LIVER}	0.48 ± 0.41*	0.83 ± 0.30	0.60 ± 0.45*	—

Values are mean ± SD.

*Significantly different from 1 ($P < 0.05$).